Atmospheric Research 212 (2018) 273–284

Contents lists available at ScienceDirect

Atmospheric Research

journal homepage: www.elsevier.com/locate/atmosres

Copula-based probabilistic characterization of precipitation extremes over North Sikkim Himalaya

Uttam P. Goswami[a], B. Hazra[a], Manish Kumar Goyal[a,b,*]

[a] Department of Civil Engineering, Indian Institute of Technology, Guwahati 781039, India
[b] Discipline of Civil Engineering, Indian Institute of Technology, Indore 453552, India

ARTICLE INFO

Keywords:
Climate change
Precipitation extreme indices
Joint return period (JRP)
Copula
CMIP5
Himalaya

ABSTRACT

Changes in climate extremes are studied based on the daily precipitation in North Sikkim Himalaya. The Coupled Model Intercomparison Project Phase 5 (CMIP5) Global Climate Models GCMs) and their Representative Concentration Pathways (RCPs) and India Meteorological Department (IMD) daily precipitation dataset are used for future and observed time periods, respectively. The purpose of this study is to examine the copula-based probabilistic behavior of precipitation extremes over the eastern Himalayan region. Seven extreme combinations were developed based on the eight defined precipitation indices. The extreme combination designates the duration, frequency and amount of heavy and weak precipitation in the same year. Statistical downscaling model (SDSM) and copulas are used for downscaling and bivariate behavior of precipitation extremes, respectively. Trend analysis result exhibits that the precipitation and its extremes (intensity, wet days, heavy precipitation days and very heavy precipitation days) are increasing significantly during 2006–2100. The spatial distributions of joint return period (JRP) of (T5, T10 and T20) marginal values are quite same during 1979–2005. In addition, the co-occurrences of heavy and weak precipitation would be more frequent in future, resulting higher risk of floods and droughts within the same year. The North Sikkim region may be at high risk of floods because precipitation extremes are increasing along with co-occurrence of flood and drought in the same year.

1. Introduction

The impact of change in climate extremes such as floods, droughts and heat waves etc. are potential disaster for society and ecosystems because of their exposure and vulnerability (Easterling et al., 2000; Mann et al., 2017; Sisco et al., 2017). The climate extremes, especially precipitation extremes may alter the frequency, intensity and duration of floods and droughts (De et al., 2005; Li et al., 2015; Singh et al., 2018), which are worse especially in agricultural dominated regions i.e., India. Correspondingly, researches on climate extremes have progressed robustly over the last decades. The Expert Team on Climate Change Detection and Indices (ETCCDI) has defined a set of climate indices to provide the widespread overview of daily temperature and precipitation (Donat et al., 2013; Sillmann et al., 2013). These extreme indices have been widely used all around the world for analyzing the changes in extremes in past (Alexander et al., 2006; Frich et al., 2002) as well as in future (Sillmann et al., 2013; Sillmann and Roeckner, 2008).

According to the Assessment Report 5 (AR5) of Intergovernmental Panel on Climate Change (IPCC) (IPCC, 2014), the likelihood of increasing climate extreme events is very soon. The increase in global mean temperature and/or climate change is expected to influence the extreme weather events, agriculture, flood and droughts and water availability (Sun et al., 2018; Zittis et al., 2017). Coupled Model Intercomparison Project Phase-5 (CMIP5) (Taylor et al., 2012) can be an important tool to address such possible changes in frequency and intensity of extreme events. The projections of meteorological extremes are uncertain and suggest robust increases in some but not all regions (Schlaepfer et al., 2017). Sillmann et al. (2013) used the CMIP5 data to analyze the precipitation indices globally during the 21st century and found an increase in extremes except for Australia, Central America, South Africa and the Mediterranean region. Donat et al. (2013) used HadEX2 and found a significant increase in precipitation extremes e.g., amount, intensity and frequency in most part of the world. Many researchers used GCMs to characterize the climate change in terms of atmospheric variables and their extremes (precipitation, temperature, evapotranspiration etc.) (Moncrieff et al., 2017; Rivière, 2011; Simpson et al., 2014). Moreover, in western Himalaya, a decrease in heavy precipitation days and consecutive wet days as well as the decreasing and inconsistent trend have been observed during 1975–2006 (Dimri

* Corresponding author at: Discipline of Civil Engineering, Indian Institute of Technology, Indore 453552, India.
E-mail address: vipmkgoyal@gmail.com (M.K. Goyal).

https://doi.org/10.1016/j.atmosres.2018.05.019
Received 22 January 2018; Received in revised form 9 May 2018; Accepted 10 May 2018
Available online 26 May 2018

and Dash, 2012). These extreme indices of precipitation and temperature can support to understand the local and global climate conditions those are amenable to all over the world.

The hydro-meteorological variables are stochastic in nature and analysis of these variables are well described by using univariate techniques (Colombo et al., 1999; Katz and Brown, 1992). In past, several probabilistic characteristics of precipitation and their extremes are investigated (Frei and Schar, 2001; Li et al., 2016; Palmer and Raisanen, 2002). These univariate estimation may under/over estimate the risk of an extreme event. Therefore, multivariate analysis of hydro-meteorological variables took place instead of univariate analysis (Grimaldi and Serinaldi, 2006). Additionally, Hashino (1985) and Yue (2001) studied the joint distribution of precipitation extremes, but, these studies are followed one assumption such as precipitation variables follow the same marginal distribution (Li et al., 2015; Zhang and Singh, 2007). To overcome this problem copula can be an important tool for multivariate analysis with its flexibility where no assumption is necessary (Salvadori and De Michele, 2004; Zhang and Singh, 2007). The introduction of copulas in hydrology has greatly facilitated the multivariate modeling (De Michele and Salvadori, 2003). Hence, the multivariate analysis techniques (copula) has been used in the different fields such as hydrology, finance, medicine etc. In recent times, different copulas are employed for multivariate analysis of annual peak snow water equivalent (SWE), annual peak flow and annual peak reservoir elevation, spatiotemporal and change in joint return periods (JRPs) of precipitation and temperature extremes, probabilistic forecasting of seasonal droughts, multivariate real-time droughts assessment, joint response of flood and drought hazards, flood frequency analysis, copula-based modeling of extreme rainfall events form 15-min precipitation dataset and bivariate rainfall frequency distribution (Bracken et al., 2018; Chen et al., 2016; Goswami et al., 2017; Li et al., 2015; Salvadori and De Michele, 2015; Sraj et al., 2015; Wang et al., 2010; Zhang and Singh, 2007; Zhang et al., 2013). From the comprehensive research, copula has found effective tool for multivariate analysis which could provide more informative knowledge of various extreme events.

Several studies focused their interest on floods and droughts all over the world based on the basis of different thresholds of precipitation (Kumar, 2016; Mathbout et al., 2018; Parthasarathy et al., 1987; Ramdas, 1972; Zaroug et al., 2014). India has experienced a number of floods and droughts which are threats to agriculture and economy of India. In India, most of the major rivers originate from glaciers such as Ganges, Brahmaputra, Indus, Teesta etc., thus the joint probabilistic nature of precipitation extremes over the glacier-fed regions is important to understand the regional response to climate change for water resources management with flood and drought controls. **In** India, a systematic study for investigation of floods and droughts within the same year has not yet been conducted. Consequently, this study focused to understand the spatiotemporal variability and joint behavior of precipitation extremes in terms of flood and drought using copula and CMIP GCMs with their respective RCPs over the North Sikkim Himalaya. To accomplish this work, firstly, downscale the precipitation at local scale using the downscaling technique (Statistical downscaling model, SDSM). Then, joint probability and return periods were analyzed for historical and projected precipitation extremes in North Sikkim Himalaya. And, finally, changes in joint return periods (CJRPs) are calculated using copula for projected scenarios.

2. Study area

The different part of the Himalayas having complex topography, climate and wind circulation which makes it a global discussion issue. The North Sikkim Himalaya up to Chugthang is chosen as the research area which lies between 25°N to 29°N latitudes and 86.25°E to 91.25°E in Sikkim, India (Fig. 1) and covers about 2587.4 km^2 area. The region, where upper region is mostly covered by snow and glaciers, and lower parts consist forest and hard rocks (Meetei et al., 2007; Singh and Goyal, 2016). The study area having pronounced steep slopes rolling between 1449 m to 6869 m m.s.l in the 92 km stretch river Teesta. The average annual precipitation is 2348.92 mm over the study area.

3. Data and methodology

3.1. Data used

The India Meteorological Department (IMD) observed gridded daily precipitation dataset at 0.5° × 0.5° spatial resolution are used for the period of 1979–2005. In addition, three CMIP5 GCMs (ESM2G, ESM2M and CM3) and their RCP scenarios (RCP2.6, RCP4.5 and RCP8.5) from CMIP5 (http://cmip-pcmdi.llnl.gov/CMIP5/) are used for various surface and atmospheric variables (Taylor et al., 2012). RCPs are the estimation of radiative forcing (RF), where RCP2.6 represents 2.6 W/m^2 and RCP4.5 represents 4.5 W/m^2 and RCP8.5 represents 8.5 W/m^2 at the end of the 21st century.

3.2. Methodology

The outputs of CMIP5 GCMs are used to project the precipitation and its extremes, but these outputs are in coarser scale, whereas the historical data are in local scale. Thus, the coarser resolution data need to downscale, for which SDSM downscaling technique is used (Wilby et al., 2002). SDSM is a statistical tool, which establish a linear regression equation between predictors (reanalysis GCM variables) and predictands (Historical dataset). Model includes two sub-models viz. conditional and unconditional, where conditional accounts wet-dry spells for establishing the regression relationship for precipitation and unconditional used for temperature. The model explains variance analysis, correlation matrix, and scatterplot, those are used for predictor selection. This relationship is used to generate the projected scenarios at local scale and further steps are shown in Fig. 3.

Firstly, the combination GCM grid-points have been constructed using Inverse distance weightage (IDW) method. Constructed combinations and GCM- grid point locations are shown in Table 1 and Fig.2 shows, how the combinations have been constructed (e.g. GCM grid-points 1, 2, 4 and 5 re-gridded and constructed 1st combination). The purpose of re-gridding is to understand the large area effect on precipitation based on the physical, climatological and hydrological significances (Goswami et al., 2017). Firstly, total 14 GCM grid-point combinations are constructed, then based on the results total 7 combinations (Table 1) are finalized, those are most significant over the region.

To analyze the climate extremes, a set of precipitation indices from ETCCDI (http://etccdi.pacificclimate.org/list_27_indices.shtml) are applied, which gives the insight of inter-annual variability of precipitation. The precipitation extremes are derived from daily precipitation to evaluate the many aspects of global climate change which include the frequency, intensity and duration of precipitation events. The precipitation extremes make a comparison in the floods and droughts extension. In addition, trends in precipitation and its extreme indices are assessed from Mann–Kendall (MK) test (Kendall, 1975; Mann, 1945) and the change in magnitude are estimated from Sen's slopes (Sen, 1968). The change in magnitude indicates that the rate of change in precipitation and its extremes every year (Table 2).

3.2.1. Copula

Copulas and its flexibility makes it useful for multivariate distributions analysis (Favre et al., 2004; Nelson, 2006; Zhang et al., 2013). The copula permits the dependence structure of random variables separately using marginal distributions. Sklar theorem (Sklar, 1959), joint distribution can be estimated using copula function and its marginal. Let$v_j = H_x(a_i)$, $j = 1, 2, 3, \ldots, m$, is the marginal cumulative distribution function (CDF) and $H_A(A)$ be the multivariate distribution

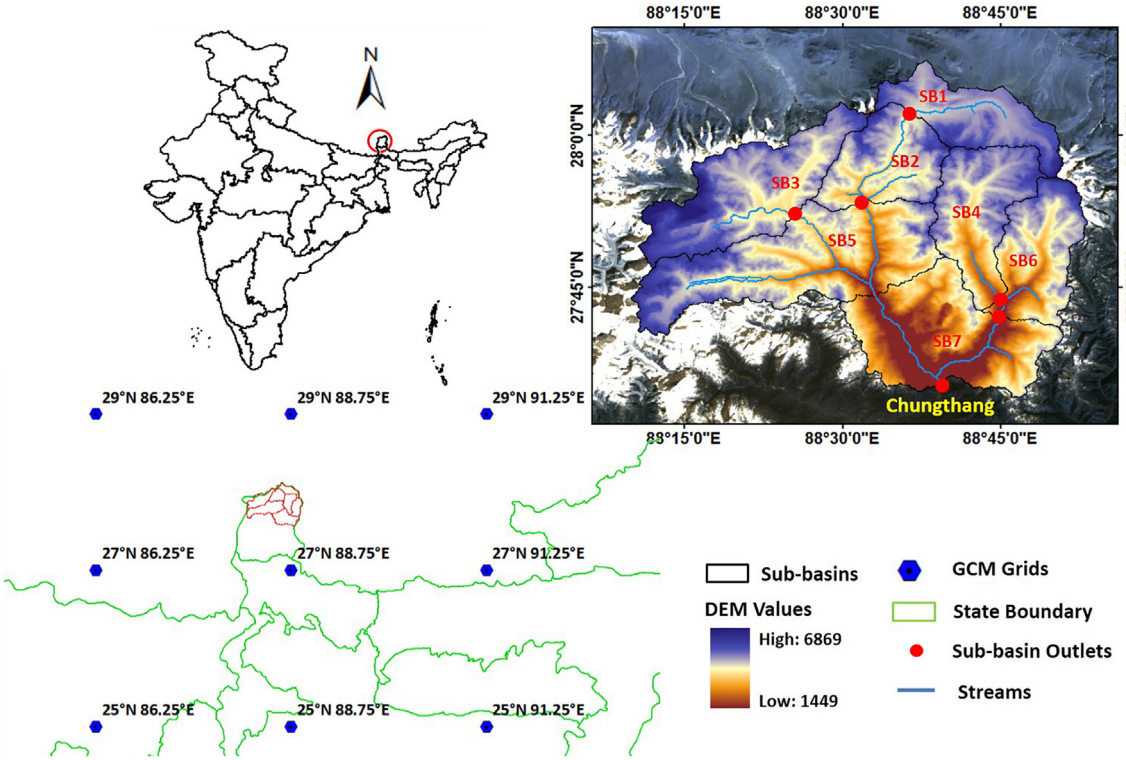

Fig. 1. Map of study area with GCM grid points over the North Sikkim Himalaya up to Chugthang.

Table 1
GCM grid-point locations and constructed combinations.

Combinations	Grid point location
Combination 1	1,2,4,5
Combination 2	2,3,5,6
Combination 3	4,5,7,8
Combination 4	5,6,8,9
Combination 5	1,2,4,5,7,8
Combination 6	2,3,5,6,8,9
Combination 7	4,5,6,7,8,9

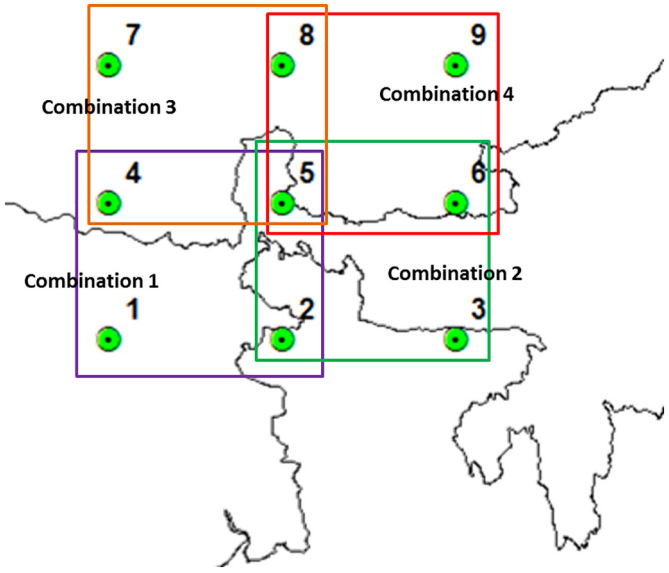

Fig. 2. Example of constructed combinations from GCM grid-points.

of $A_j j = 1, 2, 3, \ldots, m$. Thus the multivariate distribution $H_A(A)$ expressed as:

$$H_A(\mathrm{A}) = \mathrm{C}_A\{v_1, v_2, \ldots v_\mathrm{m}; \theta\} \; X \in R^d \tag{1}$$

Where, C is d-dimensional copula. The Plackett Copula (Plackett family), Gaussian Copula (Elliptical family) and Frank Copula (Archimedean family) are employed in this study. These copulas belong to three different families, which supports both positively and negatively correlated variables. Various copulas are only appropriate for positive or negative correlated variables e.g. Cook–Johnson and Gumbel-Houggard copulas (Zhang and Singh, 2007). In case of precipitation extremes, some extremes are negatively correlated and some are positively correlated too, so that these selected three copulas are suitable for this study.

Plackett Copula

$$C(u_1, u_2; \theta) = \frac{S - \sqrt{S^2 - 4u_1 u_2 \theta(\theta - 1)}}{2(\theta - 1)} \tag{2}$$

where $S = 1 + (\theta - 1)(u_1 + u_2)$ and θ lies between$(0, \infty)$.

Gaussian Copula (Elliptical family)

$$C(u_1, u_2; \theta) = \varnothing_\theta \left[\varnothing^{-1}(u_1), \varnothing^{-1}(u_2)\right] \tag{3}$$

where range of θ is$(-1, 1)$.

Frank Copula (Archimedean family)

$$C(u_1, u_2; \theta) = -\frac{1}{\theta} ln\left[1 + \frac{(e^{-\theta u1} - 1)(e^{-\theta u2} - 1)}{e^{-\theta} - 1}\right] \tag{4}$$

where range of θ is$(-\infty, \infty)$.

Where, $\varnothing^{-1}$ = inverse standard normal distribution function and.

$\varnothing_\theta$ = bivariate standard normal distribution function with θ (linear correlation coefficient).

3.2.2. Bivariate return period

Copulas are used as bivariate analysis to overcome the over and/or underestimation of risk associated with extreme events such as flood

Table 2
Definition and description of precipitation indices used in this study.

ID	Descriptive name	Indicator definition	Unit
WD	Wet days	Annual count of days when RR ≥1 mm	Days
SDII	Simple daily intensity index	Average precipitation on wet days	mm/day
R10	Heavy precipitation days	Annual count of days when RR ≥10 mm	Days
R20	Very heavy precipitation days	Annual count of days when RR ≥20 mm	Days
R95p	Very wet day precipitation	Annual total precipitation when RR ≥ 95th percentile on wet days precipitation	mm
R99p	Extremely wet day precipitation	Annual total precipitation when RR ≥99th percentile on wet days precipitation	mm
CWD	Consecutive wet days	Maximum number of consecutive wet days	Days
CDD	Consecutive dry days	Maximum number of consecutive dry days	Days

and drought. The return period of an event is defined as the time between two successive events, which provides the insights of risk analysis (Salvadori and De Michele, 2004). Here, we discuss the concept of JRP of events of pair random variables. Yue and Rasmussen (2002) have studied the physical based marginal CDF and return period of an event based on their bivariate nature. Let H(a, b) be the joint distribution function of a and b random variables and $H_{A,\ B}(a,b) = P(A \le a, B \le b)$ is the joint probability function of A and B and (a, b) is any event. While $T_{A,\ B}(a,b)$ is the JRP of an event(a, b), which can be written as:

$$T_{A,B}(a,b) = \frac{1}{1 - H_A(a) - H_B(b) + H_{A,B}(a,b)} \quad (5)$$

The change in JRP in future (2021 − 2100) is computed as:

$$\text{Changing rate} = \frac{T_{T'\{A,B\}f} - T_{T'\{A,B\}h}}{T_{T'\{A,B\}h}} \times 100\% \quad (6)$$

where, $T_T\{A,B\}f$ represents the $T_T\{A,B\}$ of future time period for different scenarios, and $T_T\{A,B\}h$ represents $T_T\{A,B\}$of historical record.

The joint extreme combination such as [CWD, CDD], [R20, SDII], [SDII, R95p], [R95p, R99p], [WD, SDII], [CDD, SDII] and [R20, R95p] are studied based on the probabilistic nature using copula. Extreme combinations are constructed based on the physical significances and Kendall's correlations. For example, the combination [CWD, CDD] presents the co-occurrence of consecutive wet days and dry days, which signifies the co-occurrence of flood and drought in the same year. The joint behavior and JRPs of precipitation extreme combinations have investigated by utilizing different copulas. An overall methodology framework applied which shows: statistical downscaling, extremes calculation and bivariate analysis of precipitation extremes (Fig. 3).

4. Results

4.1. Downscaling

A regression model was prepared by SDSM between predictors (reanalysis GCM variables) and predictands (Historical dataset). The dataset was divided into two segments for calibration (1979–1995) and validation (1996–2005) purposes. The concept of correlation and partial correlation were used to select the final predictors (Wilby et al., 2002). The coefficient of determination (R^2) is 0.75 to 0.84 for calibration and 0.71 to 0.78 for validation for different re-gridded combinations. In addition, MK and Sen's slope tests applied in annual precipitation time series. Before applying the parametric trend analysis methods (MK and Sen's slope) in annual precipitation (historical and projected) time series at catchment scale, the autocorrelation test applied to check the correlation between annual time series, resulting no statistically significant correlation in any time series obtained. The trend result indicates that the significant increasing trend in non-monsoon season, whereas no significant trend in annual and monsoon precipitation during 1979–2005. The magnitude of observed precipitation changed with +5, +14 and −6 mm/year for annual, non-monsoon and monsoon time scale, respectively.

During 2006–2100 under RCP4.5 and RCP8.5, there are the significant increasing trends at 5% significance level and no significant trend found under RCP2.6, whereas under RCP2.6 of CM3 showing

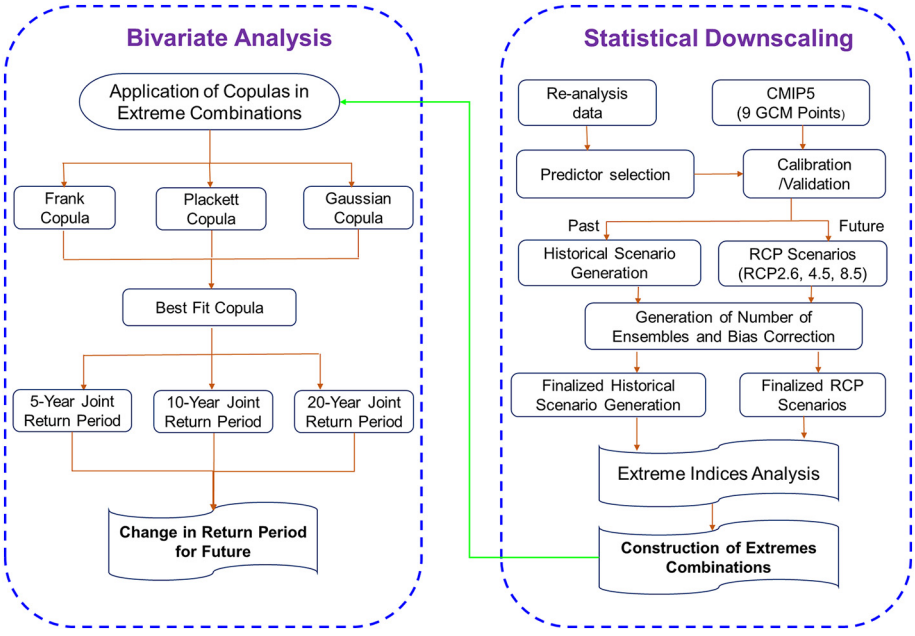

Fig. 3. Overview of proposed methodology for precipitation extremes analysis.

Table 3
Annual precipitation trends (*Z*-statistics and Slope) for three GCMs with associated RCP scenarios for the time interval of 2006–2100. Where Cs′ are combinations.

ESM2M	Parameter	C1	C2	C3	C4	C5	C6	C7
RCP2.6	Z value	**2.4**	−0.6	1.2	0.4	**2.1**	0.2	1.8
	Slope	0.6	−0.2	0.3	0.1	0.5	0.1	0.4
RCP4.5	Z value	**5.5**	**7.1**	**5.0**	**3.5**	**4.4**	**6.3**	**4.2**
	Slope	1.5	2.7	1.4	1.2	1.2	2.4	1.2
RCP8.5	Z value	**7.9**	**10.6**	**8.4**	**7.0**	**7.7**	**9.2**	**7.5**
	Slope	3.0	5.8	2.6	2.5	2.5	4.4	2.7
ESM2G	**Parameter**	**C1**	**C2**	**C3**	**C4**	**C7**	**C8**	**C11**
RCP2.6	Z value	1.4	−0.9	−0.6	−1.0	−0.8	−0.4	−0.2
	Slope	0.4	−0.3	−0.1	−0.3	−0.2	−0.1	0.0
RCP4.5	Z value	**4.9**	**6.1**	**4.2**	**2.8**	**3.6**	**5.0**	**2.4**
	Slope	1.4	2.3	1.2	0.8	0.9	1.6	0.7
RCP8.5	Z value	**7.0**	**10.3**	**7.7**	**6.5**	**7.1**	**9.9**	**7.2**
	Slope	2.3	6.2	2.7	2.2	2.2	5.3	2.4
CM3	**Parameter**	**C1**	**C2**	**C3**	**C4**	**C7**	**C8**	**C11**
RCP2.6	Z values	**6.4**	**6.2**	**7.1**	**6.5**	**6.3**	**5.9**	**7.3**
	Slopes	2.5	2.0	2.9	2.5	2.6	1.8	2.8
RCP4.5	Z values	**7.1**	**8.4**	**8.1**	**8.4**	**8.1**	**8.1**	**8.5**
	Slopes	4.1	5.3	4.6	4.3	4.4	4.6	5.0
RCP8.5	Z values	**10.5**	**12.1**	**10.5**	**11.1**	**10.6**	**11.9**	**11.0**
	Slopes	5.7	9.2	6.1	6.4	6.0	7.8	6.4

*Bold values show the significant increasing (+ve) / decreasing (−ve) trend.

significantly increasing trend (Table 3). In addition, precipitation decreased about 10–15% during 21st century as compare to historical period (1979–2005).

4.2. Precipitation extremes

The above discussed precipitation extremes are analyzed for different time scales (2006–2100, 2021–2047, 2048–2074 and 2075–2100). The average trends in precipitation indices are illustrated in Table 4 for ESM2G during 2006–2100. Similar results were obtained for ESM2M and CM3 models with different *Z*-values and slopes. The result indicates that WD, R10 and R20 of ESM2G and ESM2M showing significant increasing trend under RCP4.5 and RCP8.5, whereas CM3 shows the increasing trend for all RCPs (Table 4). Moreover, the CWD and CDD are not showing any trend except for some of the combinations. The quantification result exhibits that the WD, CWD and CDD are decreased, while heavy and very heavy precipitation days are increased during 2006–2100 with 1979–20,005. The change is about 3 to 15 days for WDs, 30 to 35 days for CWDs and 10 to15 days for CDDs for different projected scenarios. The precipitation intensity and precipitation amount (R95p and R99p) are also increased for projected scenarios. In addition, the inter-decadal result indicates that the precipitation intensity is increased and would be highest at the 80s (2075–2100).

The indices such as SDII, R95p and R99p having no significant change except for some of the combinations of SDII under RCP8.5. The spatial patterns of SDII are shown in Fig. 4 for ESM2G RCP8.5. The precipitation intensity is increased with the ranges of 1.28 to 2.25 mm/day for 20s, 1.35 to 2.09 mm/day for 50s, 1.65 to 2.87 for 80s and 1.51 to 2.32 for 21st century (Fig. 4) with reference to historical (12.17 mm/day). Moreover, R95p and R99p have been quantified and found no significant changes.

4.3. Copula results

4.3.1. Univariate and bivariate analysis

The first (GCM grid-point) combination is chosen for additional work, which illustrates the joint behavior of precipitation extremes. The joint behaviour and Kendall's tau (τ) for extreme indices are calculated (Table 5). The Kendall's tau (τ) indicates that the correlation between variable, so there is a chance that the values of both variable would be high or low if the τ value is positive or vice versa. The [CWD, CDD] and

Table 4
Mann Kendall (Z-statistics) and Sen's slope of precipitation indices for ESM2G with their RCPs, where, C's are GCM grid-point combinations.

Wet days								
Combinations		**C1**	**C2**	**C3**	**C4**	**C5**	**C6**	**C7**
RCP2.6	Z-value	0.2	−0.1	−1.5	−0.9	0.9	1.0	−0.7
	Slope	0.0	0.0	0.0	0.0	0.0	0.0	0.0
RCP4.5	*Z*-value	**3.3**	**3.1**	**2.4**	1.5	**2.2**	**2.9**	0.9
	Slope	0.1	0.1	0.1	0.1	0.1	0.1	0.0
RCP8.5	Z-value	**4.0**	**6.9**	**2.4**	**2.0**	1.7	**7.1**	**2.3**
	Slope	0.1	0.4	0.1	0.1	0.1	0.4	0.1
R10								
RCP2.6	Z-value	−1.2	−0.3	−1.5	−0.9	0.2	1.0	−0.9
	Slope	0.0	0.0	0.0	0.0	0.0	0.0	0.0
RCP4.5	Z-value	1.6	**3.2**	**2.9**	1.5	**4.1**	**3.3**	0.8
	Slope	0.0	0.1	0.1	0.0	0.1	0.1	0.0
RCP8.5	Z-value	**4.9**	**8.0**	**4.2**	**3.1**	**3.4**	**7.1**	**3.6**
	Slope	0.2	0.3	0.1	0.1	0.1	0.3	0.1
R20								
RCP2.6	Z-value	0.7	−0.5	−1.1	−1.1	−1.7	−0.7	−0.3
	Slope	0.0	0.0	0.0	0.0	0.0	0.0	0.0
RCP4.5	Z-value	0.7	1.8	1.7	1.0	**2.5**	**2.2**	1.2
	Slope	0.0	0.0	0.0	0.0	0.1	0.1	0.0
RCP8.5	Z-value	**2.2**	**7.5**	**5.1**	**2.5**	**3.4**	**6.4**	**4.0**
	Slope	0.0	0.2	0.1	0.0	0.1	0.2	0.1
CWD								
RCP2.6	Z-value	**−2.6**	−0.4	0.3	−0.7	−0.4	−0.5	−1.3
	Slope	−0.1	0.0	0.0	0.0	0.0	0.0	0.0
RCP4.5	Z-value	−0.5	1.5	0.7	0.3	0.6	1.7	0.1
	Slope	0.0	0.0	0.0	0.0	0.0	0.0	0.0
RCP8.5	Z-value	0.6	**4.8**	1.5	1.6	1.3	**4.0**	**2.8**
	Slope	0.0	0.1	0.0	0.0	0.0	0.1	0.1
CDD								
RCP2.6	Z-value	0.3	0.3	1.7	0.0	0.3	0.3	1.6
	Slope	0.0	0.0	0.1	0.0	0.0	0.0	0.1
RCP4.5	Z-value	0.7	−1.8	0.3	−0.2	−0.2	**−2.2**	0.6
	Slope	0.0	−0.1	0.0	0.0	0.0	−0.1	0.0
RCP8.5	Z-value	−1.8	0.1	0.6	0.2	−1.3	−0.3	−0.1
	Slope	−0.1	0.0	0.0	0.0	0.0	0.0	0.0

*Bold values show the significant increasing/decreasing trend.

[WD, SDII] have insignificant relations under all scenarios. [R20, SDII] and [R95p, R99p] have significant positive correlation almost for all scenarios and their Kendall's tau values are higher than 0.5 for all case except [R20, SDII] of CM3 RCP2.6 scenario. Also, [SDII, R95p] [CDD, SDII] and [R20, R95p] are highly correlated having Kendall's coefficient > 0.3 for the historical period, while less significant in projected scenarios (Table 5). The Kendall's coefficients of projected scenarios are relatively less than observed scenario. This indicates that uncertainty exists in bivariate relationships of precipitation extremes. With this consideration, further study has been carried out.

The marginal distribution of precipitation extremes are also evaluated for 5-year (T5), 10-year (T10) and 20-year (T20) return periods. The marginal values of R10 and SDII for T5, T10 and T20 return periods are slightly increased, whereas other variables such as WD, CWD and CDD are decreased in projected scenarios with respect to observed scenario. This implies that the intensity and very heavy precipitation (R10) days become stronger, while, heavy (WD and CWD) and weak (CDD) precipitation becomes less in future.

The Kendall's tau (τ) and marginal distributions are changed under projected scenarios, consequently, the joint distribution of extreme combinations may also change in future accordingly. The joint distributions are estimated for that firstly, best fit copula is chosen among Plackett, Gaussian and Frank using Akaike Information Criterion (AIC) (Akaike, 1974) and Bayesian Information Criterion (BIC). Then, based on the best fit copula, τ value and marginal distribution, the joint distribution is estimated. The joint distribution of historical and projected scenario of CWD and CDD are same, however the discrepancy in joint

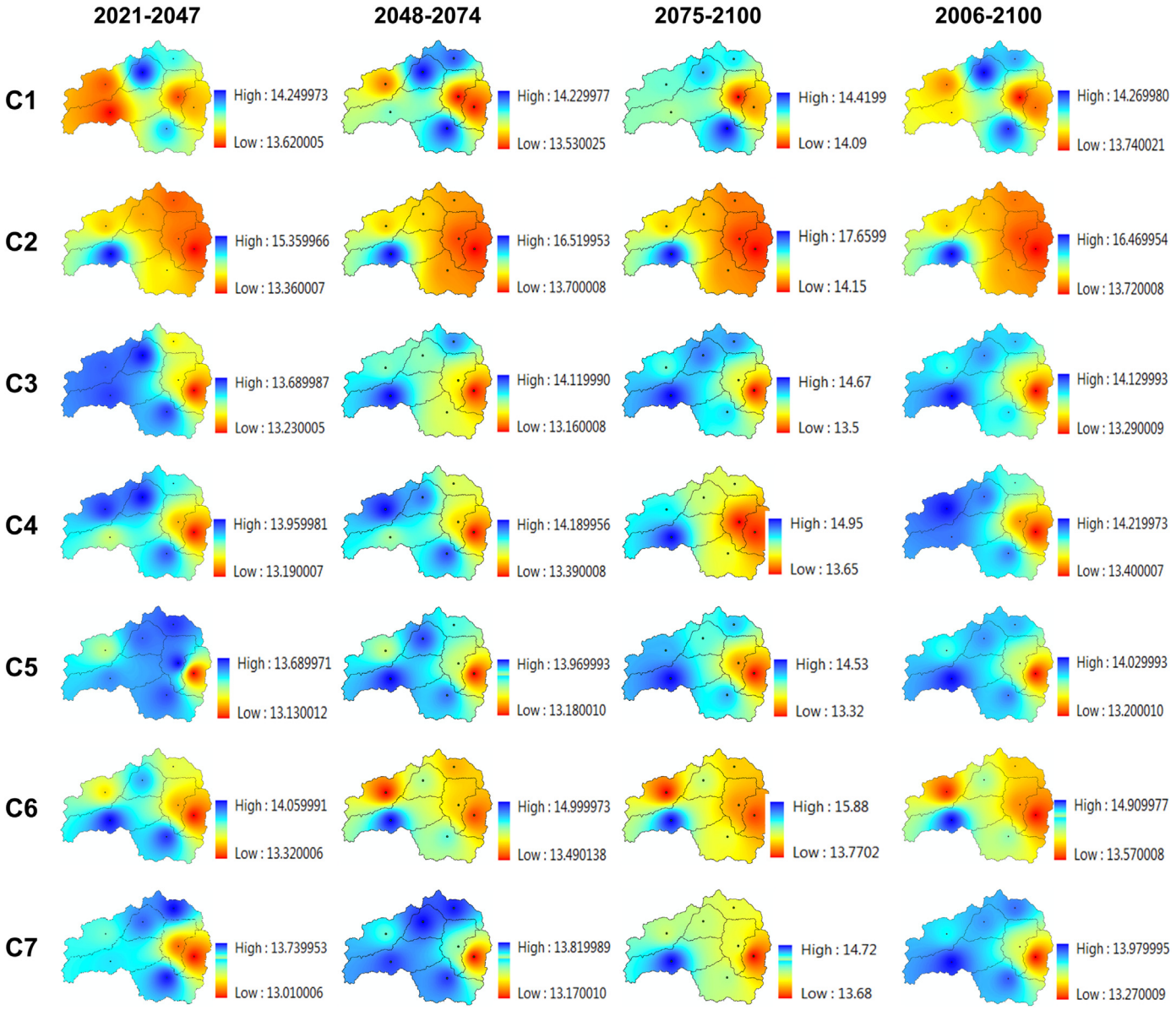

Fig. 4. Spatial variation of SDII (mm/day) for ESM2G RCP8.5 with inter-decadal scale, where C's are GCMs grid point combinations.

CDF is comparatively high when CWD and CDD values are large. The JRP of [R95p, R99p] and [R20, R95p] are quite similar, but projected scenarios are having higher joint CDF values when corresponding extreme values are large.

The non-parametric statistical distances are the distance between probability distributions (Marti et al., 2016). Here, we have used the Wasserstein (W_2), Fisher-Rao and related divergences distance. The major difference is Fisher-Rao geometry has negative curvature while Wasserstein geometry is flat and non-negative curvature. The statistical distance shows the distance between Gaussian copulas, the distances are calculated between [R95p, R99p] and [WD, SDII] extreme combinations for observed, ESM2M-RCP2.6 and ESM2M-RCP4.5 scenarios. The result highlights that 2M_RCP2.6 and 2M_RCP4.5 are closer than 2M_RCP4.5 and observed (Table 6). Here, it is surprising that since the

Table 5
The Kendall coefficients τ of extreme combination for observation and projected scenarios during 2021–2100.

Extremes	Observed	**ESM2G**			**ESM2M**			**CM3**		
		RCP2.6	RCP4.5	RCP8.5	RCP2.6	RCP4.5	RCP8.5	RCP2.6	RCP4.5	RCP8.5
[CWD, CDD]	−0.17	−0.09	0.02	0.07	0.12	0.03	0.01	−0.12	−0.06	−0.03
[R20, SDII]	0.70	0.50	0.57	0.58	0.51	0.54	0.57	0.43	0.51	0.51
[SDII, R95p]	0.43	0.08	0.18	0.03	0.16	0.11	0.19	0.14	0.21	0.17
[R95p, R99p]	0.70	0.67	0.67	0.75	0.70	0.65	0.67	0.67	0.67	0.64
[WD, SDII]	−0.48	−0.04	−0.17	−0.01	−0.23	−0.10	0.01	−0.18	0.02	0.03
[CDD, SDII]	0.30	0.02	−0.10	−0.08	0.11	0.04	−0.01	0.12	0.15	0.06
[R20, R95p]	0.46	0.12	0.19	0.06	0.13	0.03	0.23	0.26	0.34	0.02

Table 6
Statistical distances of bivariate [R95p, R99p] and [WD, SDII] extremes for ESM2M model.

Statistical distances and formulas $D(N(0,\Sigma_1),N(0,\Sigma_2))$		Distances for [R95p, R99p]		Distances for [WD, SDII]	
		D(RCP2.6, RCP4.5)	D(RCP4.5, Observed)	D(RCP2.6, RCP4.5)	D(RCP4.5, Observed)
Fisher-Rao	$\sqrt{\frac{1}{2}\sum_{i=1}^{n}(\log\lambda_i)^2}$	0.1125	0.2122	0.0271	0.411
KL(Σ_1IIΣ_2)	$\frac{1}{2}\left(log\left\|\frac{\Sigma_2}{\Sigma_1}\right\| - n + tr(\Sigma_2^{-1}\Sigma_1)\right)$	0.0067	0.025	0.0004	0.094
Jeffreys	$KL(\Sigma_1\|\Sigma_2) + KL(\Sigma_2\|\Sigma_1)$	0.0127	0.046	0.0007	0.172
Bhattacharyya	$\frac{1}{2}log\frac{\|\Sigma\|}{\sqrt{\|\Sigma_1\|\,\|\Sigma_2\|}}$	0.0016	0.006	0.0001	0.0209
Wasserstein (W_2)	$\sqrt{tr(\Sigma_1+\Sigma_2-2\sqrt{\Sigma_1^{1/2}\Sigma_2\Sigma_1^{1/2}})}$	0.0402	0.067	0.0191	0.272

λ_i Eigenvalues of ${\Sigma_1}^{-1}\Sigma_2$: $\Sigma = \frac{\Sigma_1+\Sigma_2}{2}$.

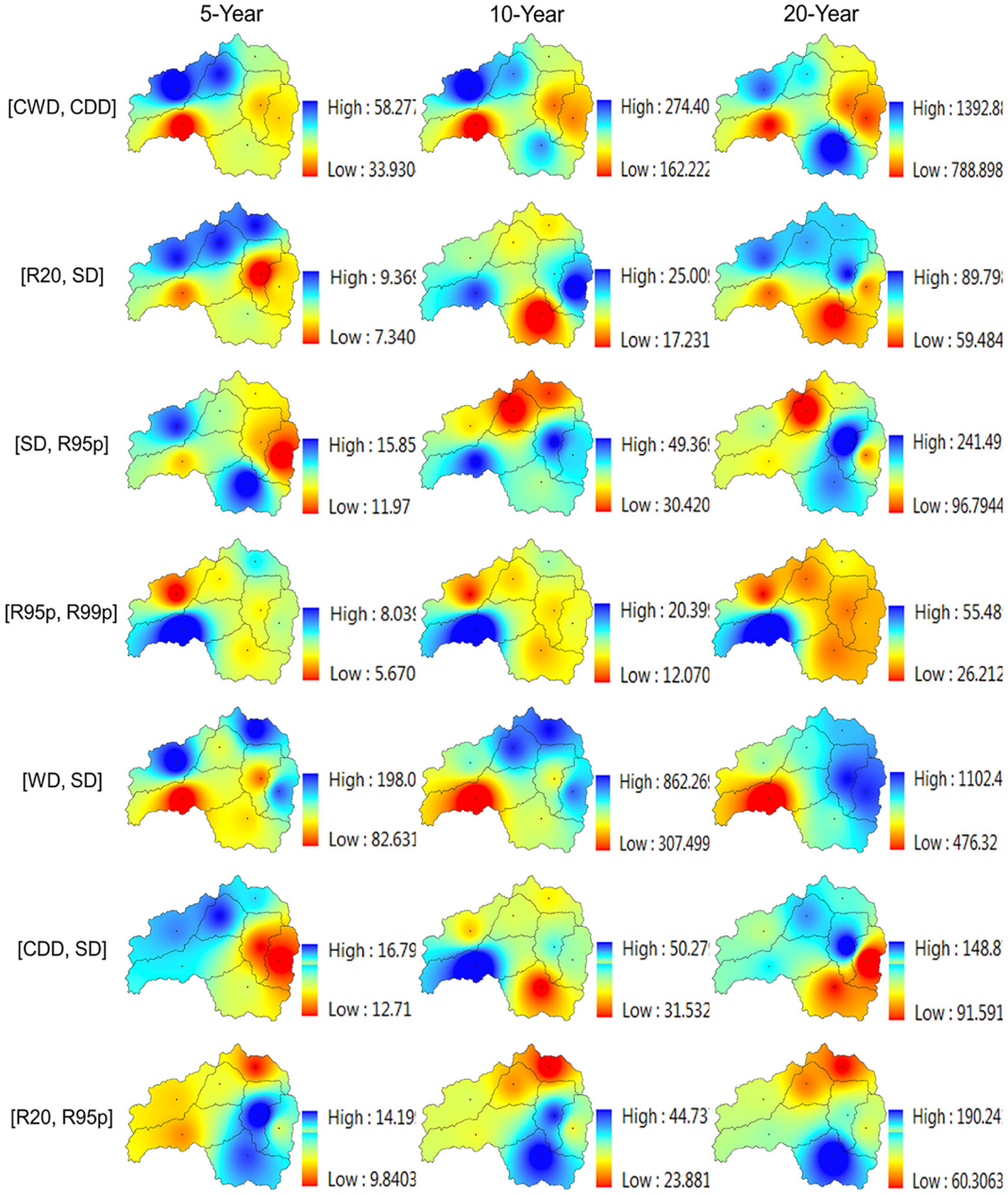

Fig. 5. Spatial distribution of observed Joint return periods (T5, T10 and T20) for precipitation extremes during 1979–2005.

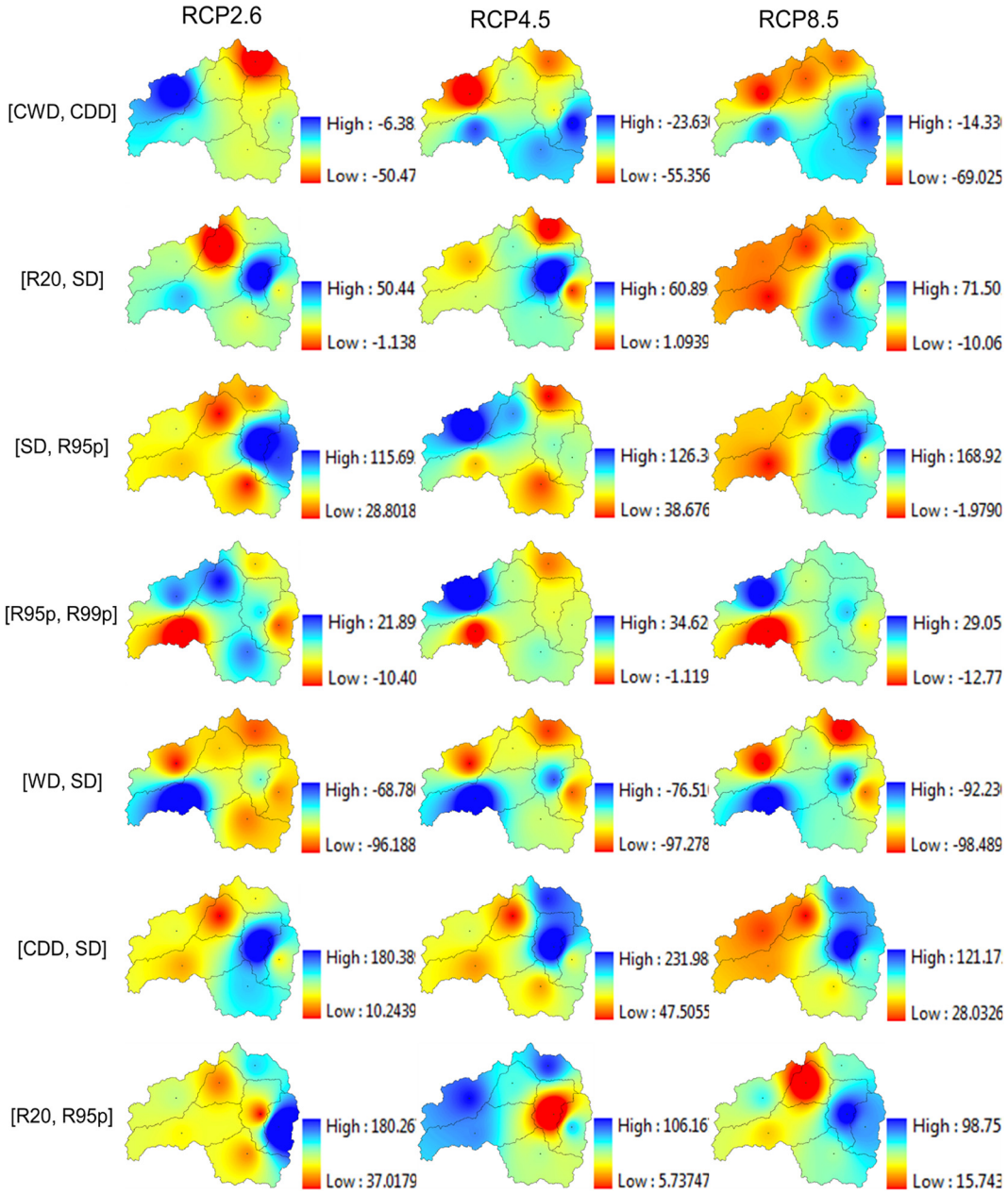

Fig. 6. The spatial distribution of changing rates (%) of T5 of extreme combinations during 2021–2100 under ESM2G with their RCPs.

strongly positive correlated (2M_RCP4.5 and Observed) are showing higher distance than less correlated scenario. The analytical formulas of statistical distances with its values are listed in Table 6.

For validation, statistical distances are calculated and found that the different scenarios showing different structures. Hence, the statistical distances (non-parametric approaches) can also be useful for bivariate analysis but this approach has some serious scaling and smoothing parameter issue which may lead to the poor description of dependence structure (Grimaldi et al., 2016; Marti et al., 2016). To overcome these issues, parametric approach (copula) is used.

4.3.2. Joint distribution and joint return-periods (JRPs) of observed (1979–2005) extreme combinations

During 1979–2005, the JRPs are investigated to understand the spatial distribution of joint behavior over the study area (Fig. 5). The result exhibits that the 5-year values of JRPs are better estimated than 10 and 20-year values. The $T_{5\ [CWD,\ CDD]}$ is ranging from 33 to 58 years which indicates that the CWD and CDD values may occur in every 33 to 58 years, which exceed their 5-year values in the same year (Fig. 5 In the upper region (sub-basins (SB) 1, 2 and 3), $T_{5\ [CWD,\ CDD]}$ is relatively high which shows the less probability of co-occurrence of excess and deficit precipitation. In case of $T_{10\ [CWD,\ CDD]}$ and $T_{20\ [CWD,\ CDD]}$ the value is much higher than $T_{5\ [CWD,\ CDD]}$ which is about > 150 years, which illustrates that the co-occurrence of excess and deficit precipitation in the same year is unlikely.

Moreover, the $T_{5\ [R20,\ SDII]}$ is quite low, ranges are 7 to 9 years, showed R20 and SDII may exceed their 5-year values in every 7 to 9 year (Fig. 5). For $T_{10\ [R20,\ SDII]}$ and $T_{20\ [R20,\ SDII]}$ the ranges from 17 to 25 years and 59 to 89 years, respectively (Fig. 5). Similarly, JRPs of [SDII, R95p] range from 11 to 16 years, 30 to 50 years and 96 to 242 years for 5, 10 and 20-year values, respectively (Fig. 5).

In Fig. 5, $T_{5\ [CDD,\ SDII]}$ is ranging from 12 to 17 years, this implies that the occurrence of drought with high intensity of precipitation in every 12–17 years. Additionally, the $T_{5\ [R20,\ R95p]}$, is ranging from 9 to 14 years, $T_{10\ [R20,\ R95p]}$, is ranging from 23 to 44 years and $T_{20\ [R20,\ R95p]}$ is ranging from 60 to 190 years with similar spatial pattern (Fig. 5). This

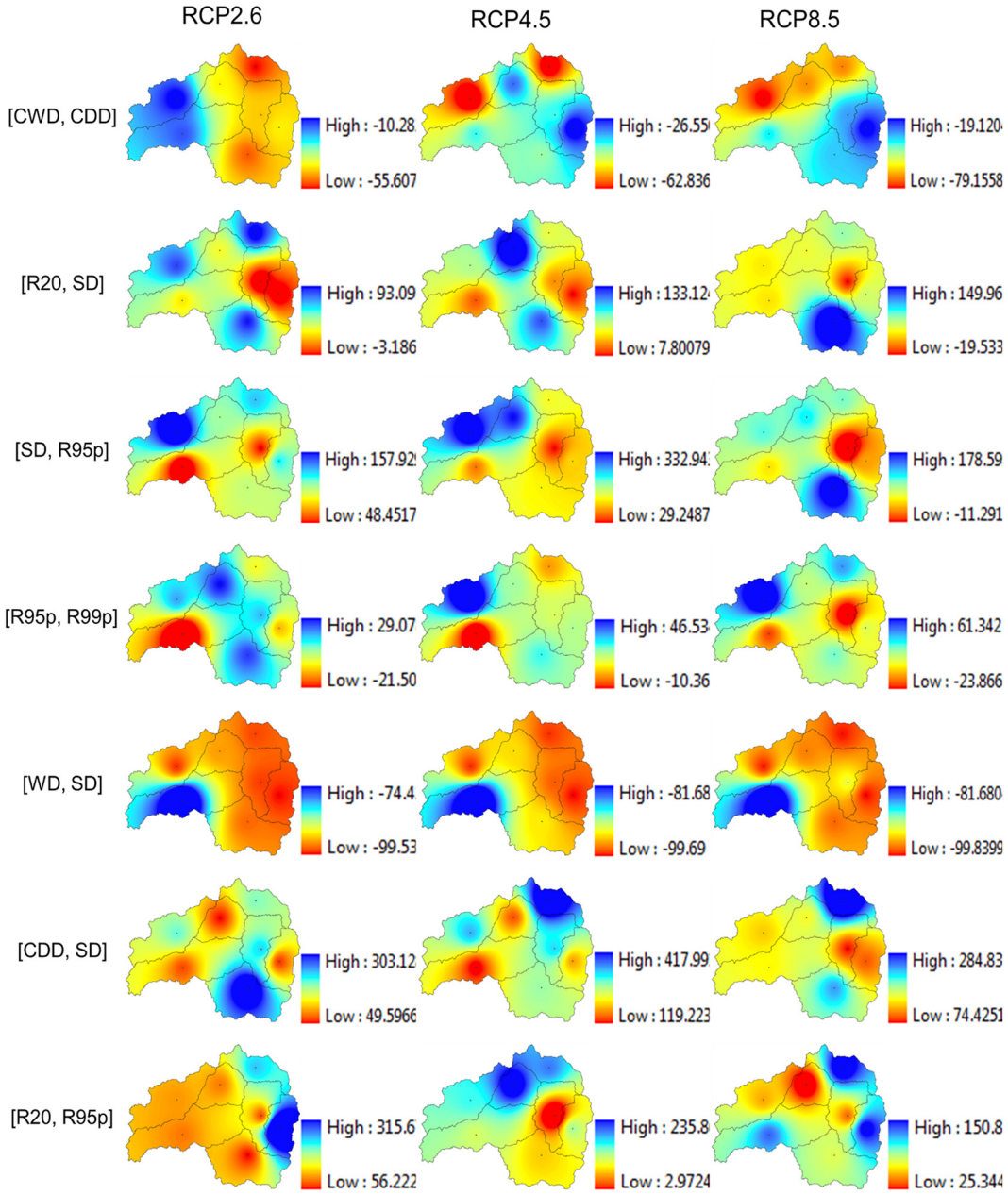

Fig. 7. The spatial distribution of changing rates (%) of T10 of extreme combinations during 2021–2100 under ESM2G with their RCPs.

shows the co-occurrence of very heavy precipitation days and heavy precipitation amount, which may increase the chances of floods.

Based on the analysis, the JRPs are spatially different for extreme combinations, whereas it is similar for 5, 10 and 20-year marginal values. The result of most of the extreme combinations shows the considerable risk of flood over the region.

4.3.3. The change in joint return period (CJRP) for projected scenarios

The joint behavior of precipitation extremes is represented as CJRPs during 2021–2100 with respect to historical 1979–2005. The CJRPs of spatial distribution are quite similar for GCM scenarios with different ranges. Therefore, only ESM2G with their RCPs results for T5, T10 and T20 are shown in Figs. 6, 7 and 8, respectively.

Fig. 6 highlights that the $T_{5\ [CWD,\ CDD]}$ is decreasing by 6 to 50% under RCP2.6, 23 to 55% under RCP4.5 and 14 to 70% under RCP8.5 scenarios. The co-occurrence of CWD and CDD decreased up to 70% for different scenarios which may exceed their 5-year values in the same year. This implies that, in future, the co-occurrence of excess and deficit precipitation are more frequent in the same year. The spatial pattern is different for RCP2.6 as compare to RCP4.5 and RCP8.5. For example, the maximum percentage change found in RCP4.5 and RCP8.5 for SB3, whereas in RCP2.6 the minimum percentage change observed in the same SB (Fig. 6).

Similarly, $T_{5\ [WD,\ SDII]}$ is decreased by 80 to 100% under different RCPs (Fig. 6), representing that once the wet days exceeds its 5-year values, precipitation intensity would also exceed its 5-year values in same year frequently. Consequently, in future, the region may face more occurrence of large precipitation with high intensity especially in upper part of the region (SB1, 2 and 3).

The $T_{5\ [R20,\ SDII]}$ is increased by up to 70% for all scenarios and SBs, except SB2 of RCP2.6 and SB2, SB3 and SB5 of RCP8.5 (Fig. 6). $T_{5\ [SDII,\ R95p]}$ is also increased by 28 to 115% for RCP2.6, 38 to 126% for RCP4.5 and 19 to 168% for RCP8.5, but in the SB5 under RCP8.5 decreased by 2% (Fig. 6). Similarly, $T_{5\ [R95p,\ R99p]}$ is also increased over the region except in SB5. These results indicate that once the extremes (R20, SDII and R95p) exceed its 5-year values, it is less probability that the other

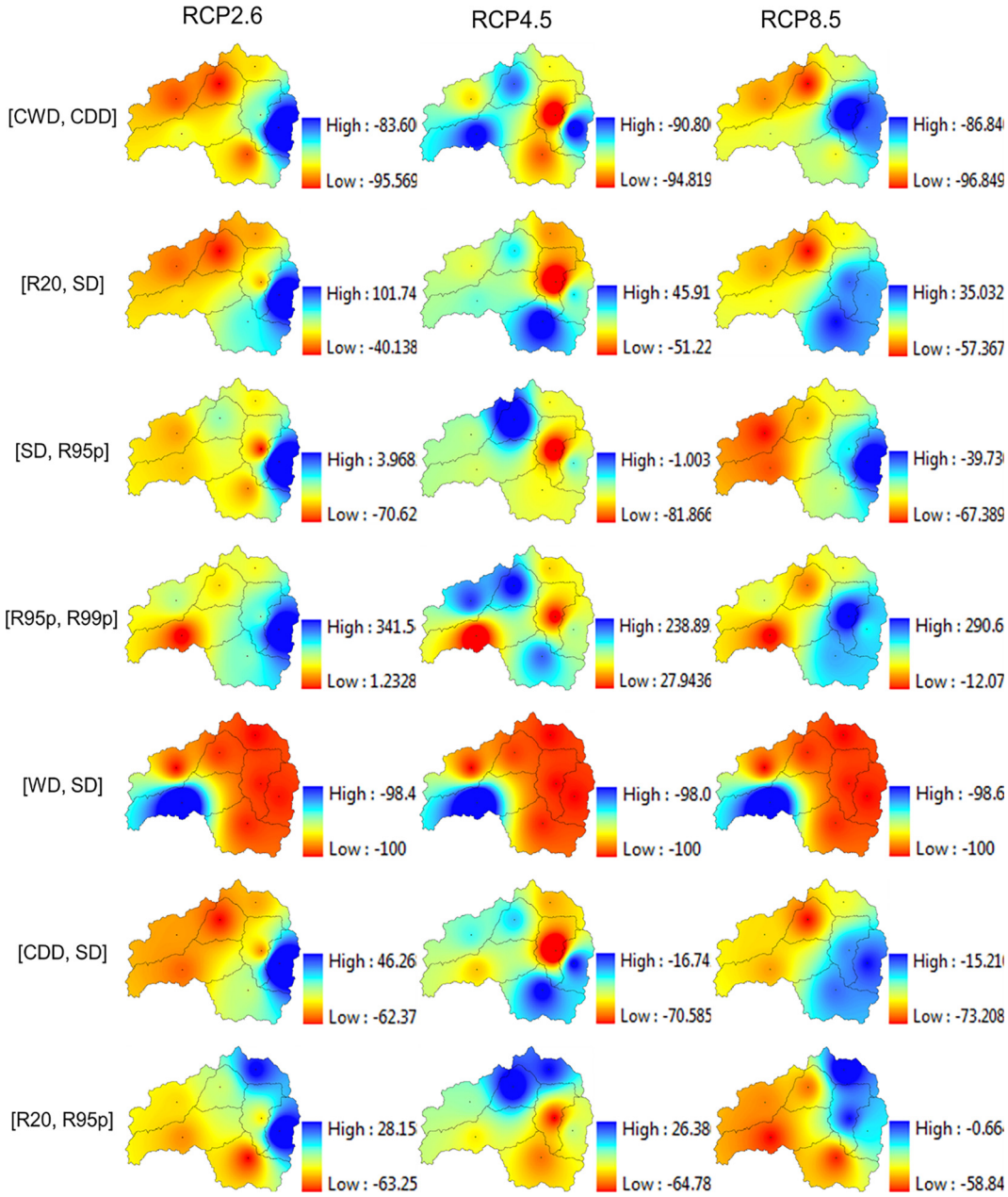

Fig. 8. The spatial distribution of changing rates (%) of T20 of extreme combinations during 2021–2100 under ESM2G with their RCPs.

extreme (SDII, R95p and R99p) will also exceed its 5-year values in same year, respectively. The $T_{5\ [CDD,\ SDII]}$ and $T_{5\ [R20,\ R95p]}$ are also increased for all scenarios, implying that, less likelihood of occurrence of floods over the region.

In addition, 10-year (Fig. 7) and 20-year (Fig. 8) CJRP have also been analyzed and found that the 5-year spatial patterns are similar for 10-year, whereas different for 20-year for some of the extreme combinations. For example, $T_{5\ [R20,\ SDII]}$ and $T_{10\ [R20,\ SDII]}$ are showing increasing percentage change except some of the sub-basins, while $T_{20\ [R20,\ SDII]}$ showing decreasing percentage change in most of the SBs. Similar pattern observed in [SDII, R95p], [CDD, SDII] and [R20, R95p]. The result exhibits that the co-occurrence of some the extreme combinations for 20-year would be more frequent as compare to 5 and 10-year.

5. Discussion

Precipitation and its extremes trends were estimated, which indicates that there is no significant trend in annual and monsoon precipitation, whereas non-monsoon precipitation shows significant increasing trend for historical time period (1979–2005). For projected scenarios, increasing trends have been observed for most of the scenarios (except RCP2.6 of ESM2G and ESM2M).

The precipitation extremes, some are increasing and some are decreasing, where trends of CWD and WD are significantly decreasing, which shows less precipitation over the region. Whereas precipitation intensity and precipitation amount as heavy and very heavy precipitation days (R95p and R99p) are increased, which show that the more intense precipitation over the region in future. This implies that the short duration heavy precipitation will occur over the region, which will contribute direct runoff resulting floods. This implies that the dominance of high extreme events as the trends are increasing or decreasing.

The spatial distributions of observed JRPs of extreme combinations are same during 1979–2005. This implies that the JRP of 5-year marginal values of any extreme combinations is high/low relative to

another place, the 10 and 20-year marginal's JRP may also be high/low in that same place. For example, the $T_{5\ [CWD,\ CDD]}$, $T_{10\ [CWD,\ CDD]}$ and $T_{20\ [CWD,\ CDD]}$ are relatively high at high elevation zones (Fig. 5).

The study area shows the heterogeneity in CJRPs of precipitation extreme combinations in future. The result highlights that the CJRPs of CWD and CDD are mainly decreased in future which indicates that the frequent co-occurrence of excess and deficit precipitation in the same year. Similarly, the CJRP of [WD, SDII] is also decreased, indicating the co-occurrence of rainy days and precipitation intensity is more frequent. This implies that North Sikkim may face heavy precipitation with high intensity resulting floods. Additionally, some of the extreme combination shows that the 5-year and 10-year CJRP increase but the 20-year CJRP decreases, indicating that the 20-year (longer duration) extremes are more frequent, whereas 5 and 10-year (relatively shorter duration) extremes are less frequent in future. But the uncertainty and biases in T20 are large, so the interpretation of change in extremes in T20 is less confident. In future, there are more possibility to occur floods and floods-droughts as joint extreme heavy precipitation increased within the same year. This study would help to prepare the proper water resources management plan during floods and droughts within the same year. In addition, the precipitation extremes are significantly changing individually and/or jointly which can create glacier hazards as the region has glaciers and number of glacial lakes.

The changing climate influences the JRP of precipitation extremes, resulting floods and/or floods and droughts in the same year in terms precipitation extreme combinations in future. The RCP8.5 scenarios are more pronounced than RCP2.6 and RCP4.5, e.g., $T_{5\ [R20,\ SD]}$ and $T_{5\ [R20,\ R95p]}$ changed dramatically under RCP8.5. It is clearly highlight that, under RCP8.5 scenario, in future the occurrence of floods as well as floods and droughts may be more frequent in the same year.

6. Conclusion

The change in precipitation and their extremes with joint behavior of extremes are investigated for the North Sikkim Himalaya using observed and CMIP5 dataset. Moreover, the CJRPs of precipitation extremes are investigated for past and future scenarios. A set of 8 precipitation extremes are used, which represent the floods and droughts with different aspects. In addition, the JRP of extreme combinations are considered, to represents the co-occurrence of precipitation extremes indices. SDSM is used to downscaling and joint behavior of precipitation extremes are investigated using copulas.

The precipitation extreme indices illustrate noticeable trend in both past and future scenarios. The spatial distribution of JRP for 5-year, 10-year and 20-year are almost similar or observed period (1979–2005). During 21st century, the co-occurrence of extreme excess and deficit precipitation in terms of consecutive wet days and dry days would be more frequent over the region, resulting floods and droughts within same year. Jointly, wet days and precipitation intensity would increase considerably in the future implying higher risk of floods during the 21st century. These changes occur may be due to change in marginal distributions and bivariate relations of extremes. Moreover, the flood and droughts would be more frequent in future in RCP8.5 scenario. These changes may create the disaster in future, so proper management plan is required for water resources systems and surroundings. In addition, a systematic plan is needed to store the water during flood condition and use stored water during drought condition, as result shows that more change of flood and droughts within the same year.

References

Akaike, H., 1974. A new look at the statistical model identification. IEEE Trans. Autom. Control 19, 716–723. http://dx.doi.org/10.1109/TAC.1974.1100705.

Alexander, L.V., Zhang, X., Peterson, T.C., Caesar, J., Gleason, B., Klein Tank, A.M.G., Haylock, M., Collins, D., Trewin, B., Rahimzadeh, F., Tagipour, A., Rupa Kumar, K., Revadekar, J., Griffiths, G., Vincent, L., Stephenson, D.B., Burn, J., Aguilar, E., Brunet, M., Taylor, M., New, M., Zhai, P., Rusticucci, M., Vazquez-Aguirre, J.L., 2006. Global observed changes in daily climate extremes of temperature and precipitation. J. Geophys. Res. Atmos. 111 (D05109). https://doi.org/10.1029/2005JD006290.

Bracken, C., Holman, K.D., Rajagopalan, B., Moradkhani, H., 2018. A Bayesian hierarchical approach to multivariate nonstationary hydrologic frequency analysis. Water Resour. Res. 54 (1), 243–255. http://dx.doi.org/10.1002/2017WR020403.

Chen, Y.D., Zhang, Q., Xiao, M., Singh, V.P., Zhang, S., 2016. Probabilistic forecasting of seasonal droughts in the Pearl River basin, China. Stoch. Environ. Res. Risk Assess. 30, 2031–2040. http://dx.doi.org/10.1007/s00477-015-1174-6.

Colombo, A.F., Etkin, D., Karney, B.W., 1999. Climate variability and the frequency of extreme temperature events for nine sites across Canada: implications for power usage. J. Clim. 12, 2490–2502. http://dx.doi.org/10.1175/1520-0442(1999).

De Michele, C., Salvadori, G., 2003. A generalized Pareto intensity-duration model of storm rainfall exploiting 2-copulas. J. Geophys. Res. 108 (D2), 4067. http://dx.doi.org/10.1029/2002JD002534.

De, U.S., Dube, R.K., Rao, G.S.P., 2005. Extreme weather events over India in the last 100 years. J. Indian Geophys. Union 9, 173–187.

Dimri, A.P., Dash, S.K., 2012. Wintertime climatic trends in the western Himalayas. Clim. Chang. 111, 775–800. http://dx.doi.org/10.1007/s10584-011-0201-y.

Donat, M.G., Alexander, L.V., Yang, H., Durre, I., Vose, R., Dunn, R.J.H., Willett, K.M., Aguilar, E., Brunet, M., Caesar, J., Hewitson, B., Jack, C., Klein Tank, A.M.G., Kruger, A.C., Marengo, J., Peterson, T.C., Renom, M., Oria Rojas, C., Rusticucci, M., Salinger, J., Elrayah, A.S., Sekele, S.S., Srivastava, A.K., Trewin, B., Villarroel, C., Vincent, L.A., Zhai, P., Zhang, X., Kitching, S., Rojas, C.O., Rusticucci, M., Salinger, J., Oria Rojas, C., Rusticucci, M., Salinger, J., Elrayah, A.S., Sekele, S.S., Srivastava, A.K., Trewin, B., Villarroel, C., Vincent, L.A., Zhai, P., Zhang, X., Kitching, S., 2013. Updated analyses of temperature and precipitation extreme indices since the beginning of the twentieth century: the HadEX2 dataset. J. Geophys. Res. Atmos. 118, 2098–2118. http://dx.doi.org/10.1002/jgrd.50150.

Easterling, D.R., Meehl, G.A., Parmesan, C., Stanley, A., Changnon, T.R.K., Mearns, L.O., 2000. Climate extremes: observations, modeling, and impacts. Science 289, 2068–2074. http://dx.doi.org/10.1126/science.289.5487.2068.

Favre, A.C., El Adlouni, S., Perreault, L., Thiemonge, N., Bobee, B., 2004. Multivariate hydrological frequency analysis using copulas. Water Resour. Res. 40, 1–12. http://dx.doi.org/10.1029/2003WR002456.

Frei, C., Schar, C., 2001. Detection probability of trends in rare events : theory and application to heavy precipitation in the alpine region. J. Clim. 14, 1568–1584. http://dx.doi.org/10.1175/1520-0442.

Frich, P., Alexander, L.V., Della-Marta, P., Gleason, B., Haylock, M., Tank Klein, A.M.G., Peterson, T., 2002. Observed coherent changes in climatic extremes during the second half of the twentieth century. Clim. Res. 19, 193–212. http://dx.doi.org/10.3354/cr019193.

Goswami, U.P., Bhargav, K., Hazra, B., Goyal, M.K., 2017. Spatiotemporal and joint probability behavior of temperature extremes over the Himalayan region under changing climate. Theor. Appl. Climatol. 1–22. http://dx.doi.org/10.1007/s00704-017-2288-1.

Grimaldi, S., Serinaldi, F., 2006. Asymmetric copula in multivariate flood frequency analysis. Adv. Water Resour. 29, 1155–1167. http://dx.doi.org/10.1016/j.advwatres.2005.09.005.

Grimaldi, S., Petroselli, A., Salvadori, G., De Michele, C., 2016. Catchment compatibility via copulas: a non-parametric study of the dependence structures of hydrological responses. Adv. Water Resour. 90, 116–133. http://dx.doi.org/10.1016/j.advwatres.2016.02.003.

Hashino, M., 1985. Formulation of the joint return period of two hydrologic variates associated with a Poisson process. J. Hydrosci. Hydraul. Eng. 3, 73–84.

IPCC, 2014. Climate change 2014: Synthesis report. In: Contribution of Working Groups I, II and III to the Fifth Assessment Report of the Intergovernmental Panel on Climate Change. Core Writing Team, R.K. Pachauri and L.A. Meyer. http://dx.doi.org/10.1017/CBO9781107415324.004.

Katz, R.W., Brown, B.G., 1992. Extreme events in changing climate variability is more important than average. Clim. Chang. 21, 289–302. http://dx.doi.org/10.1007/BF00139728.

Kendall, M.G., 1975. Rank Correlation Methods. Griffin, London.

Kumar, R., 2016. Flood hazard assessment of 2014 floods in Sonawari sub-district of Bandipore district (Jammu & Kashmir): An application of geoinformatics. Remote Sens. Appl. Soc. Environ. 4, 188–203. http://dx.doi.org/10.1016/j.rsase.2016.10.002.

Li, J., Zhang, Q., Chen, Y.D., Singh, V.P., 2015. Future joint probability behaviors of precipitation extremes across China: spatiotemporal patterns and implications for flood and drought hazards. Glob. Planet. Change 124, 107–122. http://dx.doi.org/10.1016/j.gloplacha.2014.11.012.

Li, B., Chen, Y., Chen, Z., Xiong, H., Lian, L., 2016. Why does precipitation in Northwest China show a significant increasing trend from 1960 to 2010? Atmos. Res. 167, 275–284. http://dx.doi.org/10.1016/j.atmosres.2015.08.017.

Mann, H.B., 1945. Nonparametric tests against trend. J. Econom. Soc. 13, 245–259. http://dx.doi.org/10.3982/ECTA9956.

Mann, M.E., Rahmstorf, S., Kornhuber, K., Steinman, B.A., Miller, S.K., Coumou, D., 2017. Influence of anthropogenic climate change on planetary wave resonance and extreme weather events. Sci. Rep. 7 (February). http://dx.doi.org/10.1038/srep45242.

Marti, G., Andler, S., Nielsen, F., Donnat, P., August 2-6, 2016. Optimal transport vs. Fisher-Rao distance between copulas for clustering multivariate time series. IEEE Work. Stat. Signal Process. Proc. doi:https://doi.org/10.1109/SSP.2016.7551770.

Mathbout, S., Lopez-bustins, J.A., Martin-vide, J., Bech, J., Rodrigo, F.S., 2018. Spatial and temporal analysis of drought variability at several time scales in Syria during 1961 – 2012. Atmos. Res. 200, 153–168. http://dx.doi.org/10.1016/j.atmosres.2017.09.016.

Meetei, L.I., Pattanayak, S.K., Bhaskar, A., Pandit, M.K., Tandon, S.K., 2007. Climatic

imprints in quaternary valley fill deposits of the middle Teesta valley, Sikkim Himalaya. Quat. Int. 159, 32–49. http://dx.doi.org/10.1016/j.quaint.2006.08.018.
Moncrieff, M.W., Liu, C., Bogenschutz, P., 2017. Simulation, modeling, and dynamically based parameterization of organized tropical convection for global climate models. J. Atmos. Sci. 74, 1363–1380. http://dx.doi.org/10.1175/JAS-D-16-0166.1.
Nelson, R.B., 2006. An Introduction to Copulas. vol. 137. Springer Science Business Media, pp. 2143–2150. http://dx.doi.org/10.1016/j.jspi.2006.06.045.
Palmer, T.N., Raisanen, J., 2002. Quantifying the risk of extreme seasonal precipitation events in a changing climate. Nature 415, 512–514. http://dx.doi.org/10.1038/415512a.
Parthasarathy, B., Sontakke, N.A., Monot, A.A., Kothawale, D.R., 1987. Droughts/floods in the summer monsoon season over different meteorological subdivisions of India for the period 1871-1984. Int. J. Climatol. 7, 57–70. http://dx.doi.org/10.1002/joc.3370070106.
Ramdas, L.A., 1972. Droughts and floods in India and some other countries near and far from India. In: Proc. Droughts in the Asiatic Monsoon Area Symp, Pune, pp. 91–101.
Rivière, G., 2011. A dynamical interpretation of the poleward shift of the jet streams in global warming scenarios. J. Atmos. Sci. 68, 1253–1272. http://dx.doi.org/10.1175/2011JAS3641.1.
Salvadori, G., De Michele, C., 2004. Frequency analysis via copulas: theoretical aspects and applications to hydrological events. Water Resour. Res. 40, 1–17. http://dx.doi.org/10.1029/2004WR003133.
Salvadori, G., De Michele, C., 2015. Multivariate real-time assessment of droughts via copula-based multi-site hazard trajectories and fans. J. Hydrol 526, 101–115. http://dx.doi.org/10.1016/j.jhydrol.2014.11.056.
Schlaepfer, D.R., Bradford, J.B., Lauenroth, W.K., Munson, S.M., Tietjen, B., Hall, S.A., Wilson, S.D., Duniway, M.C., Jia, G., Pyke, D.A., Lkhagva, A., Jamiyansharav, K., 2017. Climate change reduces extent of temperate drylands and intensifies drought in deep soils. Nat. Commun. 8 (14196). https://doi.org/10.1038/ncomms14196.
Sen, P.K., 1968. Estimates of the regression coefficient based on Kendall's tau. J. Am. Stat. Assoc. ISSN 63, 1379–1389. http://dx.doi.org/10.1080/01621459.1968.10480934.
Sillmann, J., Roeckner, E., 2008. Indices for extreme events in projections of anthropogenic climate change. Clim. Chang. 86, 83–104. http://dx.doi.org/10.1007/s10584-007-9308-6.
Sillmann, J., Kharin, V.V., Zwiers, F.W., Zhang, X., Bronaugh, D., 2013. Climate extremes indices in the CMIP5 multimodel ensemble: part 2. Future climate projections. J. Geophys. Res. Atmos. 118, 2473–2493. http://dx.doi.org/10.1002/jgrd.50188.
Simpson, I.R., Shaw, T.A., Seager, R., 2014. A diagnosis of the seasonally and longitudinally varying Midlatitude circulation response to global warming*. J. Atmos. Sci. 71, 2489–2515. http://dx.doi.org/10.1175/JAS-D-13-0325.1.
Singh, V., Goyal, M.K., 2016. Analysis and trends of precipitation lapse rate and extreme indices over North Sikkim eastern Himalayas under CMIP5ESM-2M RCPs experiments. Atmos. Res. 167, 34–60. http://dx.doi.org/10.1016/j.atmosres.2015.07.005.
Singh, K.S., Bonthu, S., Purvaja, R., Robin, R.S., Kannan, B.A.M., Ramesh, R., 2018. Prediction of heavy rainfall over Chennai Metropolitan City, Tamil Nadu, India: impact of microphysical parameterization schemes. Atmos. Res. 202, 219–234. http://dx.doi.org/10.1016/j.atmosres.2017.11.028.
Sisco, M.R., Bosetti, V., Weber, E.U., 2017. When do extreme weather events generate attention to climate change? Clim. Change 143 (1–2), 227–241. http://dx.doi.org/10.1007/s10584-017-1984-2.
Sklar, A., 1959. Fonctions de reprtition a n dimensions et leursmarges. Publ. Inst. Stat. Univ. Paris 8, 229–231.
Sraj, M., Bezak, N., Brilly, M., 2015. Bivariate flood frequency analysis using the copula function: a case study of the Litija station on the Sava River. Hydrol. Process. 29 (2), 225–238. http://dx.doi.org/10.1002/hyp.10145.
Sun, H., Wang, A., Zhai, J., Huang, J., Wang, Y., Wen, S., Zeng, X., Su, B., 2018. Impacts of global warming of 1.5° C and 2.0° C on precipitation patterns in China by regional climate model (COSMO-CLM). Atmos. Res. 203, 83–94. http://dx.doi.org/10.1016/j.atmosres.2017.10.024.
Taylor, K.E., Stouffer, R.J., Meehl, G.A., 2012. An overview of CMIP5 and the experiment design. Bull. Am. Meteorol. Soc. 93, 485–498. http://dx.doi.org/10.1175/BAMS-D-11-00094.1.
Wang, X., Gebremichael, M., Yan, J., 2010. Weighted likelihood copula modeling of extreme rainfall events in Connecticut. J. Hydrol. 390, 108–115. http://dx.doi.org/10.1016/j.jhydrol.2010.06.039.
Wilby, R.L., Dawson, C.W., Barrow, E.M., 2002. SDSM - a decision support tool for the assessment of regional climate change impacts. Environ. Model. Softw. 17, 147–159. http://dx.doi.org/10.1016/S1364-8152(01)00060-3.
Yue, S., 2001. The Gumbel logistic model for representing a multivariate storm event. Adv. Water Resour. 24, 179–185. http://dx.doi.org/10.1016/S0309-1708(00)00039-7.
Yue, S., Rasmussen, P., 2002. Bivariate frequency analysis: discussion of some useful concepts in hydrological application. Hydrol. Process. 16, 2881–2898. http://dx.doi.org/10.1002/hyp.1185.
Zaroug, M.A.H., Eltahir, E.A.B., Giorgi, F., 2014. Droughts and floods over the upper catchment of the Blue Nile and their connections to the timing of El Niño and La Niña events. Hydrol. Earth Syst. Sci. 18, 1239–1249. http://dx.doi.org/10.5194/hess-18-1239-2014.
Zhang, L., Singh, V.P., 2007. Bivariate rainfall frequency distributions using Archimedean copulas. J. Hydrol. 332, 93–109. http://dx.doi.org/10.1016/j.jhydrol.2006.06.033.
Zhang, Q., Li, J., Singh, V.P., Xu, C.Y., 2013. Copula-based spatio-temporal patterns of precipitation extremes in China. Int. J. Climatol. 33, 1140–1152. http://dx.doi.org/10.1002/joc.3499.
Zittis, G., Bruggeman, A., Camera, C., Hadjinicolaou, P., Lelieveld, J., 2017. The added value of convection permitting simulations of extreme precipitation events over the eastern Mediterranean. Atmos. Res. 191, 20–33. http://dx.doi.org/10.1016/j.atmosres.2017.03.002.